Topological spin textures enabling quantum transmission

Ji Zou [1,*] Stefano Bosco [2] Jelena Klinovaja [1] and Daniel Loss [1]
[1]Department of Physics, University of Basel, Klingelbergstrasse 82, 4056 Basel, Switzerland
[2]QuTech, Delft University of Technology, Lorentzweg 1, 2628 CJ Delft, The Netherlands

(Received 22 September 2024; accepted 4 September 2025; published 9 October 2025)

Quantum spintronics is an emerging field focused on developing novel applications by utilizing the quantum coherence of magnetic systems. A key challenge in this context is achieving scalable long-range quantum information transmission in magnetic systems. Here, we propose a novel transmission scheme based on topological spin textures in a hybrid architecture combining a magnetic racetrack and localized spin qubits. We demonstrate this principle by employing the domain wall (DW)—the most fundamental texture—to transport quantum signal between distant qubits. We introduce a measurement-free protocol that utilizes DW mobility to enable high-fidelity and tunable entanglement generation. Furthermore, we demonstrate that spin qubits can function as quantum stations on the racetrack, enabling flexible state transfer among fast-moving DWs on a single track. Finally, we discuss concrete material platforms to implement the proposed scheme. Our work introduces a new hybrid quantum platform that merges topological spin textures with solid-state qubits, offering a scalable architecture for quantum information processing and opening promising directions for quantum spintronics.

DOI: 10.1103/tzmn-rz7b

Topological spin textures, such as domain walls (DWs) and skyrmions, have long been explored for classical information transmission in spintronics, with landmark proposals like racetrack memory driving significant experimental advances in the control and manipulation of these textures [1,2]. In recent years, the field has experienced rapid expansion with growing interest in quantum regimes [3]. Significant efforts have been made in the community both theoretically and experimentally, including the detection of quantum magnonic states [4,5], their integration with nitrogen-vacancy (NV) centers [6,7] and superconducting qubits [8,9], and the use of topological textures as qubits for quantum devices [10–15]. However, a fundamental aspect of practical quantum spintronic devices—the reliable transmission of quantum information in magnetic systems—still remains elusive. This has, in fact, also been a critical bottleneck for many other platforms on the path to large-scale devices [16–19], prompting numerous efforts across diverse communities to overcome this challenge, such as spin shuttling [20–28] and virtual couplings enabled by cavity photons [29–40], magnons [6,41–47], Luttinger liquids [48–53], spin chains [54–59], and floating gates [60,61]. Among these, flying qubits offer a particularly promising strategy for scalable quantum architectures. Photons enable long-distance quantum communication in superconducting systems [62]. In magnetic systems, magnons serve as natural analogs and have been proposed as carriers for quantum signal transmission via real magnon propagation [63,64]. However, magnon-based schemes face fundamental limitations: Their fidelity is seriously constrained by short mean free paths [63], and they do not support universal two-qubit logic, significantly restricting their usefulness in quantum computing [64].

In this work, we propose a fully solid-state scheme for long-range quantum information transmission based on nanoscale mobile topological spin textures. We consider a hybrid system with distant spin qubits and a magnetic nanowire (racetrack), which hosts topological textures, as depicted in Fig. 1(a). We illustrate the concept by examining DWs on the track; however, this idea can also be extended to other textures such as skyrmions. This solid-state scheme

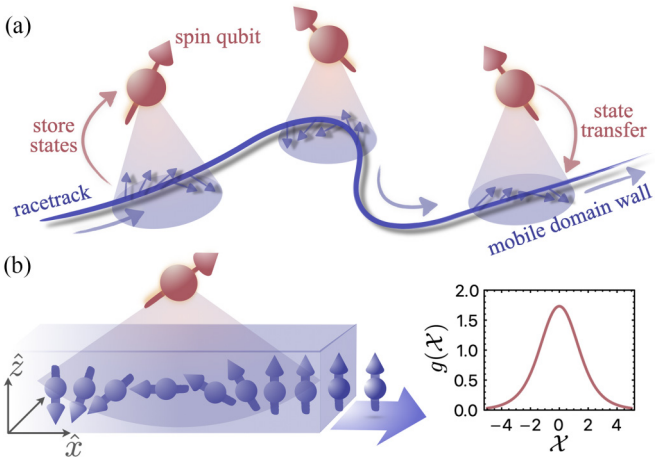

FIG. 1. (a) Schematic diagram illustrating *topological* quantum signal transmission in a hybrid system, where spin qubits interact with a magnetic nanowire hosting mobile DW textures. (b) A spin qubit interacts with a DW in the magnetic racetrack. The coupling $g(\mathcal{X})$ varies as a function of the distance $\mathcal{X}$ between the qubit and the DW.

*Contact author: ji.zou@unibas.ch

offers several interesting features. First, topological textures are solitonic excitations with inherently high mobility. This has already been demonstrated experimentally [65], enabling ultrafast quantum information transfer in a solid-state architecture. In contrast to bosonic excitations like magnons, which suffer from finite mean free paths and decay during propagation, topological textures preserve their nonlinear structures during motion [66–73], allowing for high-fidelity operations. Importantly, mobile textures can mediate long-range entangling gates between distant qubits, thus supporting universal quantum computation—overcoming a key limitation of magnon-based schemes. Furthermore, our protocol is compatible with existing racetrack memory technologies, offering a highly scalable and experimentally accessible platform. Finally, the intrinsic spin Berry phase in magnetic systems naturally induces a spin-orbit coupling, which can be harnessed to enable noise-resistant sweet spots [74] and implement dynamical decoupling [28] during transport, enhancing transfer fidelity. Our work establishes a fundamentally distinct approach to quantum information transfer using topological textures, opening up new avenues for exploration.

I. MODEL AND RACETRACK-QUBIT INTERACTION

We begin by modeling the effective interaction between spin qubits and the low-energy manifold of the DW in a magnetic wire. Let us consider a quasi-one-dimensional anisotropic ferrimagnetic nanowire, where each unit cell contains two spins, with microscopic Hamiltonian, $H = J\sum_{\langle i,j\rangle}\mathbf{S}_i\cdot\mathbf{S}_j - \mathcal{K}_z\sum_i(\hat{z}\cdot\mathbf{S}_i)^2 + \mathcal{K}_y\sum_i(\hat{y}\cdot\mathbf{S}_i)^2 - \hbar\sum_i\mathbf{h}\cdot\mathbf{S}_i$. Here, J is the antiferromagnetic exchange coupling, whereas $\mathcal{K}_z$ and $\mathcal{K}_y$ are both positive valued, representing the easy-z axis and easy-xz plane anisotropies, respectively. We assume there is a magnetic field $\mathbf{h}\equiv\gamma\mathbf{B}$ with gyromagnetic ratio γ. This system hosts DW textures described by the continuous vector field $\mathbf{n}(x)$, with $n_x(x)+in_y(x)=e^{i\phi}\mathrm{sech}\,(x-X)$ and $n_z(x)=\tanh(x-X)$ [75]. Here, ϕ and X represent the azimuthal angle and position of the DW. All distances are expressed in units of the DW width $\lambda\equiv\sqrt{J/\mathcal{K}_z}a$ with lattice spacing a.

DW textures with $\phi=0$ and π, characterized by opposite chiralities, $\mathcal{C}=(1/\pi)\int_x\hat{y}\cdot(\mathbf{n}\times\partial_x\mathbf{n})$, are energetically favorable with anisotropies $\mathcal{K}_z$ and $\mathcal{K}_y$. Other energy levels are well separated from this chirality space (the DW qubit computational space) [13]. Figure 1(b) depicts a profile with $\mathcal{C}=-1$ (at $\phi=\pi$). We quantize both ϕ and X, then project the operators $\hat{\phi}$ and $\hat{X}$ onto the two chirality states and the orbital ground state, respectively. This yields the effective quantum Hamiltonian $\mathcal{H}=-t_g\tau_x/2+\varepsilon(t)\tau_z/2$ expressed in the chirality basis $\{|\mathcal{C}=\pm1\rangle\}$. Here, $\tau_{x,z}$ are Pauli matrices, t_g is the chirality-state tunneling rate, and the detuning $\varepsilon(t)$ is given by $\varepsilon=2\hbar v(t)/\ell_{\mathrm{so}}-2\pi N\hbar S_e h_x$, where S_e is the excess spin per unit cell of the ferrimagnetic nanowire, N is the number of unit cells within the DW, and ℓ_{so} is the effective spin-orbit length arising from the intrinsic spin Berry phase. Crucially, the quantum treatment of X renormalizes the tunneling rate t_g and modifies the detuning via $v(t)=\partial_t\mathcal{X}$, where $\mathcal{X}=\langle\hat{X}\rangle$ is the expectation value of the position operator in the orbital ground state. Explicit expressions for t_g and ℓ_{so} are given in the Supplemental Material [76].

The hybrid quantum system sketched in Fig. 1(a) consists of spin qubits coupled to a racetrack. We assume the spin qubits are defined within quantum dots in a 2D nonmagnetic layer deposited adjacent to the racetrack, ensuring exchange coupling [64,77]. Thus, the interaction takes the form of $V=-J_1\sum_i|\psi(\mathbf{r}_i)|^2\mathbf{S}_i\cdot\boldsymbol{\sigma}$, where i runs over the region of the racetrack beneath the quantum dot, J_1 denotes the exchange interaction strength, $\psi(\mathbf{r}_i)$ is the orbital part of the quantum dot wavefunction, and $\boldsymbol{\sigma}$ stands for the spin qubit in the dot. To explore quantum effects, we again employ the collective coordinate quantization, projecting the dynamics onto chirality space. We find the following effective interaction between the spin qubit and the DW low-energy dynamics [76]:

$$\mathcal{V}(t)=-\mathcal{J}\,g[\mathcal{X}(t)]\,\tau_z\otimes\sigma_x, \tag{1}$$

where $\mathcal{J}=J_1|\psi|^2NS_e$ is the effective coupling strength and we assumed the wavefunction to be a constant in the dot $\psi(\mathbf{r}_i)=\psi$ for simplicity. Importantly, the time-dependent coupling envelope function is given by [76]

$$g(\mathcal{X})=\sum_{k=\pm1}\arctan[\sinh(l+k\mathcal{X})], \tag{2}$$

where l is the radius of the dot. Note that the interaction (1) is position dependent, with $\mathcal{X}(t)$ representing the time-varying distance between the DW and the center of the quantum dot, while the DW moves on the track. We depict the function $g(\mathcal{X})$ in Fig. 1(b) for $l=1$, which peaks when the DW is right beneath the dot and exhibits an exponential-decay tail, approaching $g(\mathcal{X})\to(4\sinh l)\exp\{-|\mathcal{X}(t)|\}$ as the DW moves away.

We stress that the DW motion can be controlled independently of the qubit state (chirality) [76]. For instance, a z-axis magnetic field generates a force acting on the DW position $\mathcal{X}$, driving directional motion irrespective of the chirality state $|\mathcal{C}=\pm1\rangle$. Such independent control is essential for scalable architectures.

II. ENTANGLEMENT PROTOCOL

Here we outline a *measurement-free* remote entanglement protocol based on mobile topological textures. To this end, we examine a minimal setup involving two spin qubits $\boldsymbol{\sigma}^{(i)}$ $(i=1,2)$ coupled to a racetrack containing a DW described by $\boldsymbol{\tau}$ in the chirality space. The time-dependent Hamiltonian then takes the following form:

$$\begin{aligned}\mathcal{H}(t)=&-\sum_{i=1,2}\frac{\hbar\omega_s^{(i)}}{2}\sigma_y^{(i)}-\frac{t_g}{2}\tau_x+\frac{\varepsilon(t)}{2}\tau_z\\&-\mathcal{J}\sum_{i=1,2}g[\mathcal{X}_i(t)]\sigma_x^{(i)}\tau_z,\end{aligned} \tag{3}$$

where $\omega_s^{(i)}$ is the spin qubit frequency determined by the magnetic field in the y direction and $\mathcal{X}_i(t)$ stands for the distance between the DW and the spin qubit $\boldsymbol{\sigma}^{(i)}$. In the entanglement protocol, (1) starting from trivial initial states, the DW moves beneath the first spin qubit at an optimal velocity v_0 facilitating a $\sqrt{\mathrm{iSWAP}}$ gate through time-dependent interactions (1). Then, (2) the DW shuttles from the first to the second qubit, decelerating to a suitable final velocity v_f, during which the

DW may undergo nontrivial unitary evolution U. Finally, (3) the DW approaches and interacts with the second spin qubit, realizing an iSWAP gate. These processes can be represented as the quantum circuit shown in Fig. 2(a). Importantly, this protocol operates without the need for measurements and offers flexibility to control remote entanglement between distant qubits on demand.

To illustrate the key ingredients of the scheme, we first rotate the spin axis such that the relevant part of the Hamiltonian in step (1) reads $\mathcal{H}_1(t) = -\hbar\omega_s^{(1)}\hat{\sigma}_z^{(1)}/2 - t_g\hat{\tau}_z/2 + \mathcal{J}g[\mathcal{X}_1(t)]\hat{\sigma}_x^{(1)}\hat{\tau}_x$. Here, we omit the second spin qubit, which is decoupled from both the first spin qubit and the DW. We also assume operation of the DW at the sweet spot $\varepsilon = 0$ [13] by applying a constant magnetic field $h_x = v_0/(\pi N S_e \ell_{\rm so})$. In the interaction picture and in the rotating wave approximation valid at resonance $t_g = \hbar\omega_s^{(1)}$, the time-dependent interaction yields following evolution [76]:

$$\mathcal{U} \approx \cos^2\frac{\Phi}{2} + \sin^2\frac{\Phi}{2}\hat{\sigma}_z^{(1)}\hat{\tau}_z - \frac{i}{2}\sin\Phi\big[\hat{\sigma}_x^{(1)}\hat{\tau}_x + \hat{\sigma}_y^{(1)}\hat{\tau}_y\big], \quad \text{with } \Phi(v_0) \equiv \frac{\mathcal{J}}{\hbar}\int_0^T g[\mathcal{X}(t)]\,dt = \frac{2\pi\mathcal{J}}{\hbar v_0}. \tag{4}$$

Here, we assumed that, during this step, the DW moves at a constant velocity, $\partial_t\mathcal{X}(t) = v_0$, with T representing the time required for the DW to traverse the first spin qubit. Importantly, we observe that when the phase factor Φ equals $\pi/4$, corresponding to $v_0 = 8\mathcal{J}/\hbar$, the interaction leads to an exact DW-spin qubit $\sqrt{\rm iSWAP}$ gate. With $\mathcal{J}/h \approx 100$ MHz, we have $v_0 \approx 25$ m/s, which is feasible in experiments [78–85]. Consider the initial state of the spin qubit and the DW qubit as $|\uparrow\rangle_1$ and $|\downarrow\rangle_{\rm dw}$, respectively. Following their interaction, they become entangled, yielding $(|\uparrow\rangle_1|\downarrow\rangle_{\rm dw} - i|\downarrow\rangle_1|\uparrow\rangle_{\rm dw})/\sqrt{2}$.

To entangle the two remote qubits, we slow the DW to increase its interaction time with the second qubit, enabling a hybrid DW-spin iSWAP gate. To determine the optimal final velocity v_f, we assume a reduction by $v_r \equiv v_0 - v_f$. Consequently, in step (3), the relevant time-dependent Hamiltonian becomes $\mathcal{H}_2(t) = -\hbar\omega_s^{(2)}\hat{\sigma}_z^{(2)}/2 - t_g\hat{\tau}_z/2 + (\hbar v_r/\ell_{\rm so})\hat{\tau}_x + \mathcal{J}g[\mathcal{X}_2(t)]\hat{\sigma}_x^{(2)}\hat{\tau}_x$. This Hamiltonian results in a two-qubit evolution in the interaction picture similar to Eq. (4), but importantly with a different phase factor $\tilde{\Phi} = 2\pi\mathcal{J}\cos\Theta(v_r)/\hbar v_f$, with $\cos\Theta(v_r) = \{1 + [2\hbar v_r/(\ell_{\rm so}t_g)]^2\}^{-1/2}$. The desired velocity reduction v_r is determined by

$$\frac{v_0}{v_0 - v_r} = \frac{2}{\cos\Theta(v_r)}, \tag{5}$$

where the resultant phase factor $\tilde{\Phi}$ equals $\pi/2$, corresponding to an exact iSWAP gate. We remark that the optimal final velocity v_f is not the naively expected half of the initial velocity, as shown in Fig. 2(b). Instead, it must be smaller than $v_0/2$. For a qubit frequency of 3 GHz and $\mathcal{J}/h \approx 100$ MHz, the optimal final DW velocity is determined to be 8 m/s.

While the DW velocity is reduced during its transition from the first to the second qubit in step (2), it is decoupled from both qubits, with $g(\mathcal{X}_i) = 0$, and undergoes a unitary evolution U governed by $\mathcal{H}_{\rm dw}(t)$, which depends on the changing velocity profile $v(\mathcal{X})$ shown in Fig. 2(c). Different velocity profiles lead to different unitary evolutions. Importantly, the protocol is immune to these variations. As the DW approaches the second qubit, it remains maximally entangled with the first qubit. The intermediate state can be written as $|\uparrow\rangle_1|\mathbf{n}\rangle_{\rm dw} - i|\downarrow\rangle_1|-\mathbf{n}\rangle_{\rm dw}$, with $\langle\mathbf{n}|-\mathbf{n}\rangle = \langle\downarrow|U^\dagger U|\uparrow\rangle = 0$. Assuming the second qubit is initialized in $|\uparrow\rangle_2$, the final system state after the local iSWAP operation becomes $|\Psi_{\rm final}\rangle \sim \{|\uparrow\rangle_1|\mathcal{S}^\dagger\mathbf{n}\rangle_2 - i|\downarrow\rangle_1|-\mathcal{S}^\dagger\mathbf{n}\rangle_2\} \otimes |\uparrow\rangle_{\rm dw}$, where $\mathcal{S} = {\rm diag}(1, i)$ is the phase gate. After step (3), the distant qubits form a Bell state—irrespective of the velocity profile—with the DW disentangling without projective measurements.

By leveraging the properties of the $\sqrt{\rm iSWAP}$ gate, remote entanglement generation can be controllably switched on or off by simply tuning the initial state of the DW. In particular, for initial qubit states $|\uparrow\rangle_1|\uparrow\rangle_2$, flipping the DW initial state from $|\downarrow\rangle_{\rm dw}$ to $|\uparrow\rangle_{\rm dw}$ changes the output from a Bell state to a product state $|\uparrow\rangle_1|-\mathcal{S}^\dagger\mathbf{n}\rangle_2$, all under the same protocol. Similar entanglement switching behavior occurs for other input states, as discussed in detail in the Supplemental Material [76].

A critical parameter of the remote entanglement protocol is the operation time, which comprises three parts: The durations of two local two-qubit gates and the transit time of the DW. As shown in Fig. 2(d), the total operational time resides in the nanosecond regime for qubit separations on the order

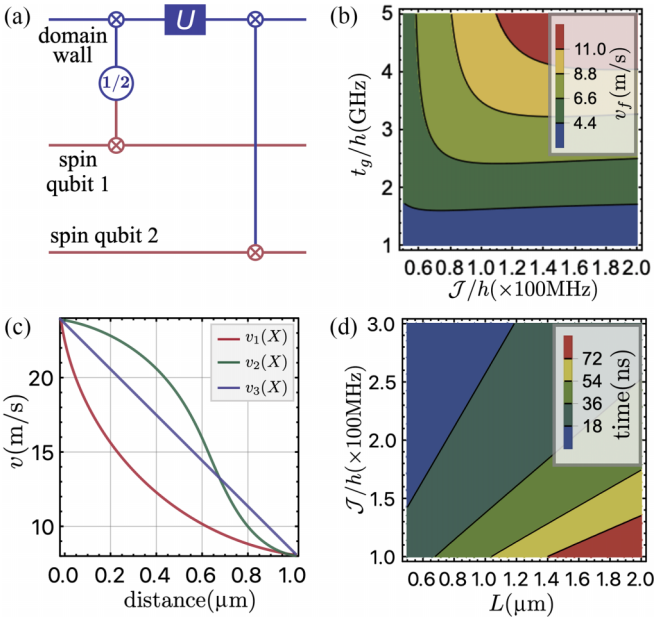

FIG. 2. (a) Quantum circuit representation of the remote entanglement protocol, which is robust to the single-qubit rotation U. (b) Optimal final DW velocity v_f as a function of the qubit frequency and the racetrack-qubit coupling. (c) Different velocity profiles on the racetrack. (d) Total operational time of the complete protocol as a function of the coupling and separation between spin qubits.

of micrometers and coupling strengths in the MHz range. The DW-spin qubit gate time, determined by $\sim\hbar l/\mathcal{J}$, is on the order of several nanoseconds for a quantum dot size of 10 nm and $\mathcal{J}/h \approx 100$ MHz. Meanwhile, the DW transit time spans tens of nanoseconds for a spin qubit separation of approximately 1 μm. Our complete protocol, therefore, operates within the rapid nanosecond regime.

Instead of varying the DW velocity to change its interaction time with the spin qubits, one may alternatively adjust the effective coupling $\mathcal{J}$ using local electric fields by repositioning the spin qubit relative to the racetrack [16]. This approach allows the realization of a $\sqrt{\text{iSWAP}}$ gate, and subsequently an iSWAP gate of the hybrid DW-spin qubit, while maintaining a constant DW velocity throughout the entire protocol.

We stress that, beyond entanglement generation, mobile DWs also enable the implementation of distant two-qubit gates, such as the $\sqrt{\text{iSWAP}}$ gate [76], offering a scalable route to universal quantum computing. This approach circumvents the limitations of magnon-mediated schemes [64] by moving the DW back and forth: The quantum state of the first qubit is transferred to the DW, which then interacts with a distant qubit to perform an entangling gate before returning to transfer the DW state back to the first qubit. This protocol effectively realizes a $\sqrt{\text{iSWAP}}$ gate between remote spin qubits.

III. ANALYSIS OF FIDELITY

To show the remote entanglement also have high fidelity $\mathcal{F}$, we now focus on both coherent and incoherent errors. The coupling between the racetrack and the spin qubit leads to the desired two-qubit interaction (1) but also induces a time-dependent magnetic field in the z direction on the spin qubit, $h_z[\mathcal{X}(t)] = \mathcal{J}\ln[\cosh(l-\mathcal{X})/\cosh(l+\mathcal{X})]$. This field causes the spin qubit axis to tilt by a small angle $\delta\theta \approx 2h_z/\hbar\omega_s$ and induces a small shift in the qubit frequency, $\delta\omega_s = \sqrt{\omega_s^2 + (2h_z/\hbar)^2} - \omega_s$.

Importantly, we find that the resultant infidelity of the hybrid DW-spin qubit gate, $\mathcal{E} = 1 - \mathcal{F}$, is always bounded from above and is analytically given by [76]

$$\mathcal{E} \leqslant 2\sin^2\frac{\delta\theta}{2} + \int_0^T \frac{dt}{2\hbar}\int_0^T \frac{ds}{2\hbar}\check{\mathcal{J}}(t)\check{\mathcal{J}}(s) \times \cos[2(\Phi(t)-\Phi(s))], \tag{6}$$

where T is again the gate time, $\Phi(t) = \mathcal{J}\int_0^t g[\mathcal{X}(\tau)]d\tau/\hbar$, and $\check{\mathcal{J}}(t) = \mathcal{J}g[\mathcal{X}(t)]\sin(\delta\omega_s t)$. The first term of Eq. (6) represents the maximal infidelity due to the tilting of the qubit axis. The (dashed) red curves in Fig. 3(a) show the corresponding value for different spin qubit frequencies ω_s as a function of the coupling $\mathcal{J}$, which is on the order of 10^{-3}. The purple curve in Fig. 3(a) illustrates the infidelity induced by the qubit frequency shift, corresponding to the second term in Eq. (6), which is estimated to be on the order of 10^{-4} to 10^{-3} for the racetrack-qubit coupling in the MHz regime.

We now focus on the infidelity induced by DW decoherence. With the DW velocity profile $v(\mathcal{X}) = v_0 + \delta v[\mathcal{X}(t)]$ in general on the racetrack, we show that the resultant infidelity

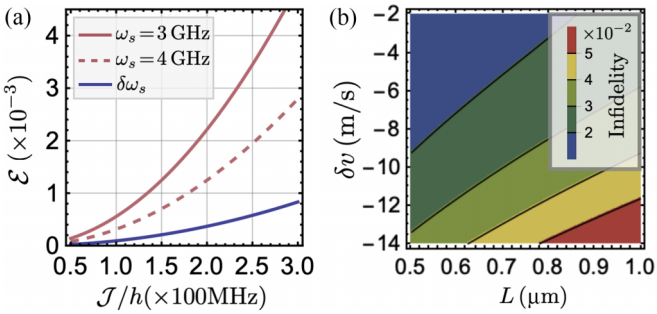

FIG. 3. (a) Two-qubit gate infidelity analysis. The (dashed) red curves illustrate the error caused by spin axis tilting for different spin qubit frequencies ω_s. The purple curve depicts the error induced by qubit frequency shifts. (b) Infidelity due to DW decoherence as a function of the velocity variation and qubit separation.

is [76]

$$\mathcal{E} \approx \frac{1}{8\hbar^2}\int_{-\infty}^{\infty}\frac{d\omega}{2\pi}S(\omega)|\mathcal{M}(\omega)|^2, \quad \text{with}$$
$$\mathcal{M} = \int_0^{\bar{T}} d\tau\, e^{-i\omega\tau}\mathbf{m}(\tau), \tag{7}$$

where $S(\omega)/\hbar^2 = \alpha N\omega\coth[\hbar\omega/(2k_BT_0)]$ is the noise spectral function with Gilbert damping α and temperature T_0, $\bar{T}$ is the total operational time, and $|\mathcal{M}(\omega)|^2$ is the effective filter function with $\mathbf{m}(t) = (\sin\theta(t)\cos\tilde{\Phi}(t), \sin\theta(t)\sin\tilde{\Phi}(t), \cos\theta(t))$. Here, $\theta(t)$ is determined by $\tan\theta(t) = -t_g\ell_{\text{so}}/[2\hbar\delta v(t)]$ and $\tilde{\Phi}(t) = \int_0^t d\tau\, t_g/[\hbar\sin\theta(\tau)]$. The detailed derivations are presented in the Supplemental Material [76]. Assuming a DW coherence time (T_2) of 0.5 μs and a constant δv for simplicity [86], we show the infidelity as a function of δv and the separation L between qubits in Fig. 3(b). The error is generally on the order of 10^{-2} for a velocity variation $\delta v \sim -10$ m/s and a qubit separation of micrometers. The infidelity from spin qubit decoherence can be estimated as $\mathcal{E} \approx \bar{T}/T_2 \approx 5\times10^{-3}$, with $\bar{T} \approx 50$ ns [see Fig. 2(d)] and spin qubit lifetime $T_2 \approx 10$ μs [16,87], which is about an order of magnitude smaller than the infidelity from DW decoherence.

We contrast our proposed scheme with magnon-based approaches in solid-state systems, which generate remote entanglement by transmitting real magnons—akin to the role of photons in optical systems. However, the conservation of magnons relies on an underlying U(1) symmetry that is easily broken by imperfections. This results in magnon decay during propagation and severely limits entanglement fidelity. In stark contrast, topological spin textures are protected by topology and remain stable during motion, making high-fidelity entanglement generation over long distances possible.

IV. QUANTUM STATION FOR RACETRACK

In the hybrid quantum system depicted in Fig. 1(a), spin qubits also nicely serve as quantum stations for the racetrack, not only storing but also facilitating the exchange of DW quantum states, which is crucial for developing a scalable quantum communication system. We consider a single spin qubit coupled to a racetrack containing multiple DWs. Assuming the quantum station—the spin qubit—is prepared

in state $|\uparrow\rangle_s$, and DW A is in a general unknown mixed state $\rho_A = \sum_i p_i |\psi_i\rangle\langle\psi_i|$, we propose moving the DW at an optimal velocity $\tilde{v} = 4\mathcal{J}/\hbar$ to store ρ_A in the spin qubit. This motion facilitates a unitary evolution that precisely executes an iSWAP gate acting on the hybrid DW-spin qubit, leading to the final state $\rho_s = \mathcal{S}^\dagger \rho_A \mathcal{S}$ of the spin qubit. By subsequently applying a phase gate, we effectively store the exact unknown state ρ_A into the spin qubit as shown in Fig. 1(a).

When another DW B on the racetrack in state $|\uparrow\rangle_B$ passes by the station at the velocity $\tilde{v}$ at later time, the time-dependent interaction with the spin qubit again realizes another iSWAP gate, leading to the final state of DW B as $\rho_B = \mathcal{S}^\dagger \rho_A \mathcal{S}$. Therefore, the spin qubit facilitates the transfer of quantum states between fast-moving DWs on the same racetrack, enabling quantum information exchange among different topological spin textures on the same racetrack, which would otherwise be a challenging task. In the dual picture, DWs also act as *mobile* quantum stations for spin qubits, facilitating long-distance spin-qubit state transfer. We note that by moving the first DW at a slower velocity or adjusting the coupling $\mathcal{J}$ with local electric fields to enable a hybrid DW-spin qubit $\sqrt{\text{iSWAP}}$ gate, we can also entangle different DWs on the same track.

V. DISCUSSION

A key requirement for realizing DW-based quantum information transport is maintaining nanoscale DW widths for reliable qubit encoding. Atomically thin magnetic multilayers such as Co/Ni and CoFeB are promising candidates due to their strong magnetic anisotropy, supporting sub-10-nm DWs and demonstrated velocities exceeding 100 m/s [65]. Two-dimensional van der Waals magnets, such as Fe_3GeTe_2, also offer attractive properties, including low damping for improved coherence and reduced current requirements for DW motion, minimizing heating [88].

In parallel, spin qubits confined in silicon or germanium quantum dots provide a compatible and scalable platform for integration with racetracks [77]. Micromagnets are already widely used in spin qubit manipulation [16], and in the present context, such qubits can couple to DW via dipole or exchange interactions. Together, these material platforms offer a feasible and promising route for realizing the proposed architecture.

ACKNOWLEDGMENTS

We thank Banabir Pal and Stuart Parkin for insightful discussions. This work was supported by the Georg H. Endress Foundation and by the Swiss National Science Foundation, NCCR SPIN (Grant No. 51NF40-180604).

DATA AVAILABILITY

No data were created or analyzed in this study.

[1] S. S. P. Parkin, M. Hayashi, and L. Thomas, Magnetic domain-wall racetrack memory, Science **320**, 190 (2008).
[2] A. Fert, V. Cros, and J. Sampaio, Skyrmions on the track, Nat. Nanotechnol. **8**, 152 (2013).
[3] H. Yuan, Y. Cao, A. Kamra, R. A. Duine, and P. Yan, Quantum magnonics: When magnon spintronics meets quantum information science, Phys. Rep. **965**, 1 (2022).
[4] D. Lachance-Quirion, S. P. Wolski, Y. Tabuchi, S. Kono, K. Usami, and Y. Nakamura, Entanglement-based single-shot detection of a single magnon with a superconducting qubit, Science **367**, 425 (2020).
[5] A.-L. E. Römling, A. Vivas-Viaña, C. S. Muñoz, and A. Kamra, Resolving nonclassical magnon composition of a magnetic ground state via a qubit, Phys. Rev. Lett. **131**, 143602 (2023).
[6] M. Fukami, J. C. Marcks, D. R. Candido, L. R. Weiss, B. Soloway, S. E. Sullivan, N. Delegan, F. J. Heremans, M. E. Flatté, and D. D. Awschalom, Magnon-mediated qubit coupling determined via dissipation measurements, Proc. Natl. Acad. Sci. USA **121**, e2313754120 (2024).
[7] J. Zou, S. Zhang, and Y. Tserkovnyak, Bell-state generation for spin qubits via dissipative coupling, Phys. Rev. B **106**, L180406 (2022).
[8] Y. Tabuchi, S. Ishino, A. Noguchi, T. Ishikawa, R. Yamazaki, K. Usami, and Y. Nakamura, Coherent coupling between a ferromagnetic magnon and a superconducting qubit, Science **349**, 405 (2015).
[9] M. Kounalakis, G. E. W. Bauer, and Y. M. Blanter, Analog quantum control of magnonic cat states on a chip by a superconducting qubit, Phys. Rev. Lett. **129**, 037205 (2022).
[10] C. Psaroudaki and C. Panagopoulos, Skyrmion qubits: A new class of quantum logic elements based on nanoscale magnetization, Phys. Rev. Lett. **127**, 067201 (2021).
[11] J. Xia, X. Zhang, X. Liu, Y. Zhou, and M. Ezawa, Universal quantum computation based on nanoscale skyrmion helicity qubits in frustrated magnets, Phys. Rev. Lett. **130**, 106701 (2023).
[12] X.-F. Pan, P.-B. Li, X.-L. Hei, X. Zhang, M. Mochizuki, F.-L. Li, and F. Nori, Magnon-skyrmion hybrid quantum systems: Tailoring interactions via magnons, Phys. Rev. Lett. **132**, 193601 (2024).
[13] J. Zou, S. Bosco, B. Pal, S. S. P. Parkin, J. Klinovaja, and D. Loss, Quantum computing on magnetic racetracks with flying domain wall qubits, Phys. Rev. Res. **5**, 033166 (2023).
[14] G. Qu, J. Zou, D. Loss, and T. Hirosawa, Density matrix renormalization group study of domain wall qubits, Phys. Rev. B **112**, 054432 (2025).
[15] S. Takei and M. Mohseni, Quantum control of topological defects in magnetic systems, Phys. Rev. B **97**, 064401 (2018).
[16] G. Burkard, T. D. Ladd, A. Pan, J. M. Nichol, and J. R. Petta, Semiconductor spin qubits, Rev. Mod. Phys. **95**, 025003 (2023).
[17] G. Burkard, M. J. Gullans, X. Mi, and J. R. Petta, Superconductor–semiconductor hybrid-circuit quantum electrodynamics, Nat. Rev. Phys. **2**, 129 (2020).
[18] A. Blais, A. L. Grimsmo, S. M. Girvin, and A. Wallraff, Circuit quantum electrodynamics, Rev. Mod. Phys. **93**, 025005 (2021).

[19] L. Vandersypen, H. Bluhm, J. Clarke, A. Dzurak, R. Ishihara, A. Morello, D. Reilly, L. Schreiber, and M. Veldhorst, Interfacing spin qubits in quantum dots and donors—Hot, dense, and coherent, npj Quantum Inf. **3**, 34 (2017).

[20] T. Fujita, T. A. Baart, C. Reichl, W. Wegscheider, and L. M. K. Vandersypen, Coherent shuttle of electron-spin states, npj Quantum Inf. **3**, 22 (2017).

[21] A. Mills, D. Zajac, M. Gullans, F. Schupp, T. Hazard, and J. Petta, Shuttling a single charge across a one-dimensional array of silicon quantum dots, Nat. Commun. **10**, 1063 (2019).

[22] J. Yoneda, W. Huang, M. Feng, C. H. Yang, K. W. Chan, T. Tanttu, W. Gilbert, R. Leon, F. Hudson, K. Itoh *et al.*, Coherent spin qubit transport in silicon, Nat. Commun. **12**, 4114 (2021).

[23] B. Jadot, P.-A. Mortemousque, E. Chanrion, V. Thiney, A. Ludwig, A. D. Wieck, M. Urdampilleta, C. Bäuerle, and T. Meunier, Distant spin entanglement via fast and coherent electron shuttling, Nat. Nanotechnol. **16**, 570 (2021).

[24] A. Zwerver, S. Amitonov, S. De Snoo, M. Madzik, M. Rimbach-Russ, A. Sammak, G. Scappucci, and L. Vandersypen, Shuttling an electron spin through a silicon quantum dot array, PRX Quantum **4**, 030303 (2023).

[25] A. Noiri, K. Takeda, T. Nakajima, T. Kobayashi, A. Sammak, G. Scappucci, and S. Tarucha, A shuttling-based two-qubit logic gate for linking distant silicon quantum processors, Nat. Commun. **13**, 5740 (2022).

[26] I. Seidler, T. Struck, R. Xue, N. Focke, S. Trellenkamp, H. Bluhm, and L. R. Schreiber, Conveyor-mode single-electron shuttling in Si/SiGe for a scalable quantum computing architecture, npj Quantum Inf. **8**, 100 (2022).

[27] V. Langrock, J. A. Krzywda, N. Focke, I. Seidler, L. R. Schreiber, and Ł. Cywiński, Blueprint of a scalable spin qubit shuttle device for coherent mid-range qubit transfer in disordered Si/SiGe/SiO_2, PRX Quantum **4**, 020305 (2023).

[28] S. Bosco, J. Zou, and D. Loss, High-fidelity spin qubit shuttling via large spin-orbit interactions, PRX Quantum **5**, 020353 (2024).

[29] X. Mi, M. Benito, S. Putz, D. M. Zajac, J. M. Taylor, G. Burkard, and J. R. Petta, A coherent spin–photon interface in silicon, Nature (London) **555**, 599 (2018).

[30] A. J. Landig, J. V. Koski, P. Scarlino, U. Mendes, A. Blais, C. Reichl, W. Wegscheider, A. Wallraff, K. Ensslin, and T. Ihn, Coherent spin–photon coupling using a resonant exchange qubit, Nature (London) **560**, 179 (2018).

[31] F. Borjans, X. Croot, X. Mi, M. Gullans, and J. Petta, Resonant microwave-mediated interactions between distant electron spins, Nature (London) **577**, 195 (2020).

[32] C. X. Yu, S. Zihlmann, J. C. Abadillo-Uriel, V. P. Michal, N. Rambal, H. Niebojewski, T. Bedecarrats, M. Vinet, É. Dumur, M. Filippone *et al.*, Strong coupling between a photon and a hole spin in silicon, Nat. Nanotechnol. **18**, 741 (2023).

[33] P. Harvey-Collard, J. Dijkema, G. Zheng, A. Sammak, G. Scappucci, and L. M. Vandersypen, Coherent spin-spin coupling mediated by virtual microwave photons, Phys. Rev. X **12**, 021026 (2022).

[34] P.-Q. Jin, M. Marthaler, A. Shnirman, and G. Schön, Strong coupling of spin qubits to a transmission line resonator, Phys. Rev. Lett. **108**, 190506 (2012).

[35] S. Bosco, P. Scarlino, J. Klinovaja, and D. Loss, Fully tunable longitudinal spin-photon interactions in Si and Ge quantum dots, Phys. Rev. Lett. **129**, 066801 (2022).

[36] M. Benito, J. R. Petta, and G. Burkard, Optimized cavity-mediated dispersive two-qubit gates between spin qubits, Phys. Rev. B **100**, 081412 (2019).

[37] A. Warren, E. Barnes, and S. E. Economou, Long-distance entangling gates between quantum dot spins mediated by a superconducting resonator, Phys. Rev. B **100**, 161303 (2019).

[38] S. E. Nigg, A. Fuhrer, and D. Loss, Superconducting grid-bus surface code architecture for hole-spin qubits, Phys. Rev. Lett. **118**, 147701 (2017).

[39] M. Trif, V. N. Golovach, and D. Loss, Spin dynamics in InAs nanowire quantum dots coupled to a transmission line, Phys. Rev. B **77**, 045434 (2008).

[40] G. Burkard and A. Imamoglu, Ultra-long-distance interaction between spin qubits, Phys. Rev. B **74**, 041307 (2006).

[41] L. Trifunovic, F. L. Pedrocchi, and D. Loss, Long-distance entanglement of spin qubits via ferromagnet, Phys. Rev. X **3**, 041023 (2013).

[42] B. Flebus and Y. Tserkovnyak, Entangling distant spin qubits via a magnetic domain wall, Phys. Rev. B **99**, 140403 (2019).

[43] J. Zou, S. K. Kim, and Y. Tserkovnyak, Tuning entanglement by squeezing magnons in anisotropic magnets, Phys. Rev. B **101**, 014416 (2020).

[44] W. Xiong, M. Tian, G.-Q. Zhang, and J. Q. You, Strong long-range spin-spin coupling via a Kerr magnon interface, Phys. Rev. B **105**, 245310 (2022).

[45] T. c. v. Neuman, D. S. Wang, and P. Narang, Nanomagnonic cavities for strong spin-magnon coupling and magnon-mediated spin-spin interactions, Phys. Rev. Lett. **125**, 247702 (2020).

[46] Z. Xue, J. Zou, C. Cai, G. E. Bauer, and T. Yu, Directional entanglement of spin-orbit locked nitrogen-vacancy centers by magnons, arXiv:2505.07325.

[47] S. Driessen, J. Zou, E. Thingstad, J. Klinovaja, and D. Loss, Robust tripartite entanglement generation via correlated noise in spin qubits, arXiv:2506.20466.

[48] G. Yang, C.-H. Hsu, P. Stano, J. Klinovaja, and D. Loss, Long-distance entanglement of spin qubits via quantum Hall edge states, Phys. Rev. B **93**, 075301 (2016).

[49] T. M. Stace, C. H. W. Barnes, and G. J. Milburn, Mesoscopic one-way channels for quantum state transfer via the quantum Hall effect, Phys. Rev. Lett. **93**, 126804 (2004).

[50] J. Viennot, J. Palomo, and T. Kontos, Stamping single wall nanotubes for circuit quantum electrodynamics, Appl. Phys. Lett. **104**, 113108 (2014).

[51] S. Bosco and D. P. DiVincenzo, Transmission lines and resonators based on quantum Hall plasmonics: Electromagnetic field, attenuation, and coupling to qubits, Phys. Rev. B **100**, 035416 (2019).

[52] S. J. Elman, S. D. Bartlett, and A. C. Doherty, Long-range entanglement for spin qubits via quantum Hall edge modes, Phys. Rev. B **96**, 115407 (2017).

[53] S. Bosco, D. DiVincenzo, and D. Reilly, Transmission lines and metamaterials based on quantum Hall plasmonics, Phys. Rev. Appl. **12**, 014030 (2019).

[54] S. Bose, Quantum communication through an unmodulated spin chain, Phys. Rev. Lett. **91**, 207901 (2003).

[55] M. Friesen, A. Biswas, X. Hu, and D. Lidar, Efficient multi-qubit entanglement via a spin bus, Phys. Rev. Lett. **98**, 230503 (2007).

[56] F. K. Malinowski, F. Martins, T. B. Smith, S. D. Bartlett, A. C. Doherty, P. D. Nissen, S. Fallahi, G. C. Gardner, M. J. Manfra,

C. M. Marcus *et al.*, Fast spin exchange across a multielectron mediator, Nat. Commun. **10**, 1196 (2019).
[57] R. Sánchez, G. Granger, L. Gaudreau, A. Kam, M. Pioro-Ladrière, S. A. Studenikin, P. Zawadzki, A. S. Sachrajda, and G. Platero, Long-range spin transfer in triple quantum dots, Phys. Rev. Lett. **112**, 176803 (2014).
[58] T. A. Baart, T. Fujita, C. Reichl, W. Wegscheider, and L. M. K. Vandersypen, Coherent spin-exchange via a quantum mediator, Nat. Nanotechnol. **12**, 26 (2017).
[59] H. Qiao, Y. P. Kandel, S. Fallahi, G. C. Gardner, M. J. Manfra, X. Hu, and J. M. Nichol, Long-distance superexchange between semiconductor quantum-dot electron spins, Phys. Rev. Lett. **126**, 017701 (2021).
[60] L. Trifunovic, O. Dial, M. Trif, J. R. Wootton, R. Abebe, A. Yacoby, and D. Loss, Long-distance spin-spin coupling via floating gates, Phys. Rev. X **2**, 011006 (2012).
[61] M. Serina, C. Kloeffel, and D. Loss, Long-range interaction between charge and spin qubits in quantum dots, Phys. Rev. B **95**, 245422 (2017).
[62] M. Ansmann, H. Wang, R. C. Bialczak, M. Hofheinz, E. Lucero, M. Neeley, A. D. O'Connell, D. Sank, M. Weides, J. Wenner *et al.*, Violation of Bell's inequality in Josephson phase qubits, Nature (London) **461**, 504 (2009).
[63] M. Fukami, D. R. Candido, D. D. Awschalom, and M. E. Flatté, Opportunities for long-range magnon-mediated entanglement of spin qubits via on- and off-resonant coupling, PRX Quantum **2**, 040314 (2021).
[64] B. Heténi, A. Mook, J. Klinovaja, and D. Loss, Long-distance coupling of spin qubits via topological magnons, Phys. Rev. B **106**, 235409 (2022).
[65] S. Parkin and S.-H. Yang, Memory on the racetrack, Nat. Nanotechnol. **10**, 195 (2015).
[66] *Topology in Magnetism*, edited by J. Zang, V. Cros, and A. Hoffmann (Springer International Publishing, Cham, Switzerland, 2018).
[67] J. Zou, S. Zhang, and Y. Tserkovnyak, Topological transport of deconfined hedgehogs in magnets, Phys. Rev. Lett. **125**, 267201 (2020).
[68] X. S. Wang, A. Qaiumzadeh, and A. Brataas, Current-driven dynamics of magnetic hopfions, Phys. Rev. Lett. **123**, 147203 (2019).
[69] Y. Tserkovnyak, J. Zou, S. K. Kim, and S. Takei, Quantum hydrodynamics of spin winding, Phys. Rev. B **102**, 224433 (2020).
[70] Y. Liu, W. Hou, X. Han, and J. Zang, Three-dimensional dynamics of a magnetic hopfion driven by spin transfer torque, Phys. Rev. Lett. **124**, 127204 (2020).
[71] J. Zou, S. K. Kim, and Y. Tserkovnyak, Topological transport of vorticity in Heisenberg magnets, Phys. Rev. B **99**, 180402 (2019).
[72] D. Jones, J. Zou, S. Zhang, and Y. Tserkovnyak, Energy storage in magnetic textures driven by vorticity flow, Phys. Rev. B **102**, 140411 (2020).
[73] Y. Tserkovnyak and J. Zou, Quantum hydrodynamics of vorticity, Phys. Rev. Res. **1**, 033071 (2019).
[74] S. Bosco, B. Heténi, and D. Loss, Hole spin qubits in Si FinFETs with fully tunable spin-orbit coupling and sweet spots for charge noise, PRX Quantum **2**, 010348 (2021).
[75] S. K. Kim and O. Tchernyshyov, Mechanics of a ferromagnetic domain wall, J. Phys.: Condens. Matter **35**, 134002 (2023).
[76] See Supplemental Material at http://link.aps.org/supplemental/10.1103/tzmn-rz7b for (1) deriving the effective coupling between spin qubits and domain walls, (2) controlling domain wall motion independently of qubit state, (3) effective unitary evolution under the racetrack-qubit interaction, (4) discussion of different initial states and the robustness of the entanglement protocol, (5) universality of the distant two-qubit logic, and (6) detailed derivations of protocol fidelity.
[77] D. Loss and D. P. DiVincenzo, Quantum computation with quantum dots, Phys. Rev. A **57**, 120 (1998).
[78] O. Gomonay, T. Jungwirth, and J. Sinova, High antiferromagnetic domain wall velocity induced by Néel spin-orbit torques, Phys. Rev. Lett. **117**, 017202 (2016).
[79] K.-S. Ryu, L. Thomas, S.-H. Yang, and S. Parkin, Chiral spin torque at magnetic domain walls, Nat. Nanotechnol. **8**, 527 (2013).
[80] S.-H. Yang, K.-S. Ryu, and S. Parkin, Domain-wall velocities of up to 750 m s^{-1} driven by exchange-coupling torque in synthetic antiferromagnets, Nat. Nanotechnol. **10**, 221 (2015).
[81] K.-J. Kim, S. K. Kim, Y. Hirata, S.-H. Oh, T. Tono, D.-H. Kim, T. Okuno, W. S. Ham, S. Kim, G. Go, Y. Tserkovnyak, A. Tsukamoto, T. Moriyama, K.-J. Lee, and T. Ono, Fast domain wall motion in the vicinity of the angular momentum compensation temperature of ferrimagnets, Nat. Mater. **16**, 1187 (2017).
[82] S.-H. Yang, R. Naaman, Y. Paltiel, and S. S. P. Parkin, Chiral spintronics, Nat. Rev. Phys. **3**, 328 (2021).
[83] Y. Guan, X. Zhou, F. Li, T. Ma, S.-H. Yang, and S. S. P. Parkin, Ionitronic manipulation of current-induced domain wall motion in synthetic antiferromagnets, Nat. Commun. **12**, 5002 (2021).
[84] R. Bläsing, T. Ma, S.-H. Yang, C. Garg, F. K. Dejene, A. T. N'Diaye, G. Chen, K. Liu, and S. S. P. Parkin, Exchange coupling torque in ferrimagnetic Co/Gd bilayer maximized near angular momentum compensation temperature, Nat. Commun. **9**, 4984 (2018).
[85] Y. Yoshimura, K.-J. Kim, T. Taniguchi, T. Tono, K. Ueda, R. Hiramatsu, T. Moriyama, K. Yamada, Y. Nakatani, and T. Ono, Soliton-like magnetic domain wall motion induced by the interfacial Dzyaloshinskii–Moriya interaction, Nat. Phys. **12**, 157 (2016).
[86] C. Psaroudaki, E. Peraticos, and C. Panagopoulos, Skyrmion qubits: Challenges for future quantum computing applications, Appl. Phys. Lett. **123**, 260501 (2023).
[87] Y.-H. Wu, L. C. Camenzind, P. Bütler, I. K. Jin, A. Noiri, K. Takeda, T. Nakajima, T. Kobayashi, G. Scappucci, H.-S. Goan *et al.*, Simultaneous high-fidelity single-qubit gates in a spin qubit array, arXiv:2507.11918.
[88] W. Zhang, T. Ma, B. K. Hazra, H. Meyerheim, P. Rigvedi, Z. Yin, A. K. Srivastava, Z. Wang, K. Gu, S. Zhou *et al.*, Current-induced domain wall motion in a van der Waals ferromagnet Fe_3GeTe_2, Nat. Commun. **15**, 4851 (2024).